

# Energy & Environmental Science

Accepted Manuscript



This is an *Accepted Manuscript*, which has been through the Royal Society of Chemistry peer review process and has been accepted for publication.

*Accepted Manuscripts* are published online shortly after acceptance, before technical editing, formatting and proof reading. Using this free service, authors can make their results available to the community, in citable form, before we publish the edited article. We will replace this *Accepted Manuscript* with the edited and formatted *Advance Article* as soon as it is available.

You can find more information about *Accepted Manuscripts* in the [Information for Authors](#).

Please note that technical editing may introduce minor changes to the text and/or graphics, which may alter content. The journal's standard [Terms & Conditions](#) and the [Ethical guidelines](#) still apply. In no event shall the Royal Society of Chemistry be held responsible for any errors or omissions in this *Accepted Manuscript* or any consequences arising from the use of any information it contains.

## ARTICLE

Cite this: DOI: 10.1039/x0xx00000x

Received 00th January 2012,

Accepted 00th January 2012

DOI: 10.1039/x0xx00000x

www.rsc.org/

## Nanocrystalline Ni<sub>5</sub>P<sub>4</sub>: A hydrogen evolution electrocatalyst of exceptional efficiency in both alkaline and acidic media

A. B. Laursen<sup>a</sup>, K. R. Patraju<sup>a</sup>, M. J. Whitaker<sup>a</sup>, M. Retuerto<sup>a</sup>, T. Sarkar<sup>a</sup>, N. Yao<sup>b</sup>, K. V. Ramanujachary<sup>c</sup>, M. Greenblatt<sup>a,\*</sup>, G. C. Dismukes<sup>a,\*</sup>

Producing hydrogen (H<sub>2</sub>) by splitting water with fossil-free electricity, is considered a grand challenge for developing sustainable energy systems and a carbon dioxide free source of renewable H<sub>2</sub>. Renewable H<sub>2</sub> may be produced from water by electrolysis with either low efficiency alkaline electrolyzers that suffer 50-65% losses, or by more efficient acidic electrolyzers with rare platinum group metal catalysts (Pt). Consequently, research has focused on developing alternative, cheap, and robust catalysts made from earth-abundant elements. Here, we show that crystalline Ni<sub>5</sub>P<sub>4</sub> evolves H<sub>2</sub> with geometric electrical to chemical conversion efficiency on par with Pt in strong acid (33 mV/dec Tafel slope and -62 mV overpotential at -100 mA/cm<sup>2</sup> in 1 M H<sub>2</sub>SO<sub>4</sub>). The conductivity of Ni<sub>5</sub>P<sub>4</sub> microparticles is sufficient to allow fabrication of electrodes without conducting binders by pressing pellets. Significantly, no catalyst degradation is seen in short term studies at current densities of -10 mA/cm<sup>2</sup>, equivalent to ~10% solar photoelectrical conversion efficiency. The realization of a noble metal-free catalyst performing on par with Pt in both strong acid and base offers a key step towards industrially relevant electrolyzers competing with conventional H<sub>2</sub> sources.

### 1. Introduction

Although H<sub>2</sub> can be produced by electrochemical water-splitting, commercial alkaline electrolyzers rely on metallic nickel (Ni) electrodes that have low efficiencies and suffer electrochemical corrosion, which are acceptable only because of the low cost of Ni metal. Recent advances include the use of electrodeposited NiMo alloy catalysts with yet undisclosed stability/longevity under commercial conditions. Commercial Proton Exchange Membrane (PEM)-type electrolyzers use platinum (Pt) particles on carbon, the archetypical catalyst for the H<sub>2</sub> evolution reaction (HER). On pure Pt [110] the reaction has the highest efficiency, being thermodynamically reversible in acids, and each additional 29 mV of applied potential increases the current ten-fold (Tafel slope of 29 mV/dec), which is the lowest electrical loss reported<sup>1</sup>. However, platinum group metals (PGM) are among the scarcest elements on Earth (Pt is 10<sup>5</sup> [10<sup>6</sup>] times scarcer than Ni [P]) and very expensive<sup>2,3</sup>. Consequently, research has focused on developing alternative HER catalysts from earth-abundant elements that are affordable, yet retain the high conversion efficiency of PGMs during extended operation. Another need is for stability under alkaline operation for compatibility with metal oxide catalysts for the Oxygen Evolution Reaction (OER), which typically are not stable in acid electrolytes. In acidic electrolytes the most efficient earth-abundant HER catalysts are molybdenum sulfides<sup>4-6</sup>, a porous Mo-C-N composite<sup>7</sup>, and Ni<sub>2</sub>P nanoparticles<sup>8</sup> (*vide infra*) with low overpotentials of  $\eta = -257$ ,  $-178$ , &  $-134$  mV vs. the Reversible Hydrogen Electrode (RHE is referenced to the measured pH, see ESI) at a current density of  $j = -10$  mA/cm<sup>2</sup>, respectively and low Tafel slopes of 40, 36, & 46 mV/dec respectively). Supported CoP nanoparticles were

recently reported to exhibit the best HER efficiency in acid until now (overpotential of -74 mV vs. RHE at -10 mA/cm<sup>2</sup>). Transition metal phosphides of Fe<sup>9-12</sup>, Ni<sup>13,8,14-16</sup>, Co<sup>17-19</sup>, Mo<sup>20-23</sup>, and W<sup>24</sup> as well as other advances in earth-abundant HER catalysts have been reviewed recently<sup>25</sup>. At alkaline pH, amorphous NiMo nanoparticles (alloy) are considered the state-of-the-art in efficiency, with an overpotential of -82 mV vs. RHE at -10 mA/cm<sup>2</sup><sup>26</sup>, although they degrade in acid<sup>8</sup>. Some molecular nickel organophosphine complexes that model hydrogenases are exceptionally active HER catalysts with turnover frequencies (TOFs) up to 10<sup>5</sup> s<sup>-1</sup> (1.2 M H<sub>2</sub>O in CH<sub>3</sub>CN)<sup>27</sup>, however, they decompose during catalysis (<5% in 0.5 hr in dry CH<sub>3</sub>CN). Theoretical calculations by Liu and Rodriguez predicted that the [001] facet of the nickel phosphide, Ni<sub>2</sub>P should be more a more active HER catalyst than Pt<sup>28</sup>. Based in part on this prediction, we set out to evaluate all 7 structurally and stoichiometrically distinct Ni<sub>x</sub>P<sub>y</sub> phases that are stable below 800°C. Recently, Popczun et al.<sup>8</sup> described the HER activity of Ni<sub>2</sub>P nanoparticles (NPs) predominantly expressing the [001] facet and confirmed the high activity of this material, although still less active than Pt<sup>28</sup>. Nanoparticulate Ni<sub>5</sub>P<sub>4</sub> has previously been shown to be an efficient anode material in lithium-ion batteries<sup>29,30</sup>, although its catalytic properties have not been reported.

Herein, we report the synthesis of nanocrystalline Ni<sub>5</sub>P<sub>4</sub> and describe its superior efficiency as an HER catalyst as well as significantly improved electrochemical corrosion resistance compared to Ni<sub>2</sub>P NPs. Ni<sub>5</sub>P<sub>4</sub> has an HER electrocatalytic geometric activity on par with bulk Pt catalysts and exhibits minimal loss in activity after 16 hr of H<sub>2</sub> evolution in both 1 M

H<sub>2</sub>SO<sub>4</sub> and 1 M NaOH—an unique attribute among PGM-free HER catalysts.

## 2. Results:

**2.1. Synthesis & Characterization:** We synthesized micron sized particles of Ni<sub>5</sub>P<sub>4</sub> (Ni<sub>5</sub>P<sub>4</sub> MPs) and Ni<sub>2</sub>P NPs as single phase crystalline particles by adapting previously reported solvothermal methods<sup>31,32</sup>. Special attention to prevent formation of the other 6 crystalline phases of nickel phosphides was necessary to achieve high purity.

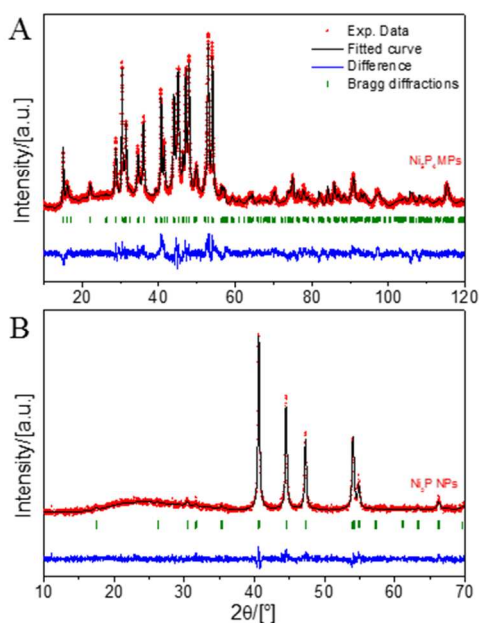


Fig. 1 PXRD analysis of Ni<sub>5</sub>P<sub>4</sub> (A) and Ni<sub>2</sub>P (B) comparing the observed (+), Rietveld refinement calculated curve (black) and difference (blue) at room temperature. The

Bragg positions (vertical lines) correspond to the crystallographic reflections. The Ni<sub>5</sub>P<sub>4</sub> structure is refined in a hexagonal unit-cell, space group P63mc (#186), with unit-cell parameters  $a = 6.78822(15)$  Å,  $c = 11.0086(4)$  Å. No additional peaks, indicative of impurities are observed, showing that Ni<sub>5</sub>P<sub>4</sub> is the only crystalline component (details in S.I.). The small differences between fit and data are due to the size range of the particles from 20 nm–1.8 μm, see HRTEM. The Ni<sub>2</sub>P NP structure refinement used the Ni<sub>2</sub>P reference pattern (PDF 03-065-3544), refining the following parameters: zero-point, scale factor, positional and thermal factors, and unit-cell parameters. Graphs are vertically displaced for clarity.

Rietveld refinement of the Ni<sub>5</sub>P<sub>4</sub> reference pattern to the Ni<sub>5</sub>P<sub>4</sub> MPs PXRD pattern shown in Fig. 1A, shows that both the peak positions and intensities agree with the fit, establishing that Ni<sub>5</sub>P<sub>4</sub> is the only crystalline component within the ~2 % detection limit. The Scherrer equation indicates an average particle size of ~20 nm. Rietveld refinement of the PXRD also confirmed Ni<sub>2</sub>P as phase-pure nanoparticles (NPs) with a particle size of 5–6 nm from the Scherrer equation, see Fig. 1B.

HRTEM further confirmed both the Ni<sub>5</sub>P<sub>4</sub> phase from lattice spacings (see Table S4, ESI) and the NP crystallite size range 5–20 nm (Fig. 2B). Ni<sub>5</sub>P<sub>4</sub> NPs were found to have fused together to form larger spherical MPs, size 0.3–1.8 μm (Fig. 2A). HRTEM shows that individual particles are encapsulated in a thin ( $1.1 \pm 0.5$  nm), amorphous shell. The transmission dependence on atomic number, suggests that this shell is amorphous carbon, likely produced from breakdown of the organophosphine precursor, as reported previously for similar syntheses<sup>29</sup>.

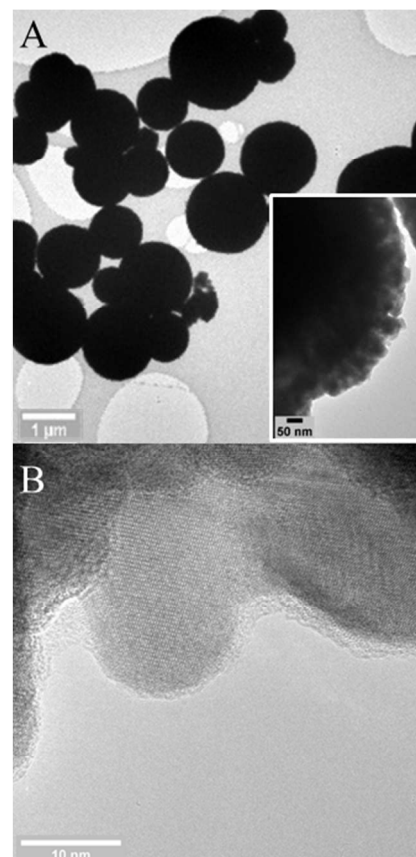


Fig. 2 TEM image of Ni<sub>5</sub>P<sub>4</sub> MPs before catalysis. (A) TEM image at low magnification (insert) zoom in on MP edge showing the particles nano-roughness. (B) HRTEM image of a single nanoparticle of MP particle agglomerate.

**2.2. Electrochemical activity measurement:** As Ni<sub>5</sub>P<sub>4</sub> converts into Ni<sub>2</sub>P when heated above 350°C<sup>33</sup>, the procedure used by Popczun et al.<sup>8</sup> to prepare thin-film electrodes by sintering Ni<sub>2</sub>P onto Ti-foil could not be applied here. Instead, electrodes were made by pressing 50 mg of catalyst into a 6 mm diameter pellet (at 5 tons) and sealing it in epoxy so that only the top surface of the electrode contacted the solution (see Methods & ESI). The electric conductivity of the Ni<sub>5</sub>P<sub>4</sub> MP pellets are measured by the 4-point probe technique. The obtained resistivity of 6.3 μΩ·m and using a representative pellet thickness of 480 μm and geometric area of 0.021 cm<sup>2</sup> the electrode resistance attributable to the pellet design was only

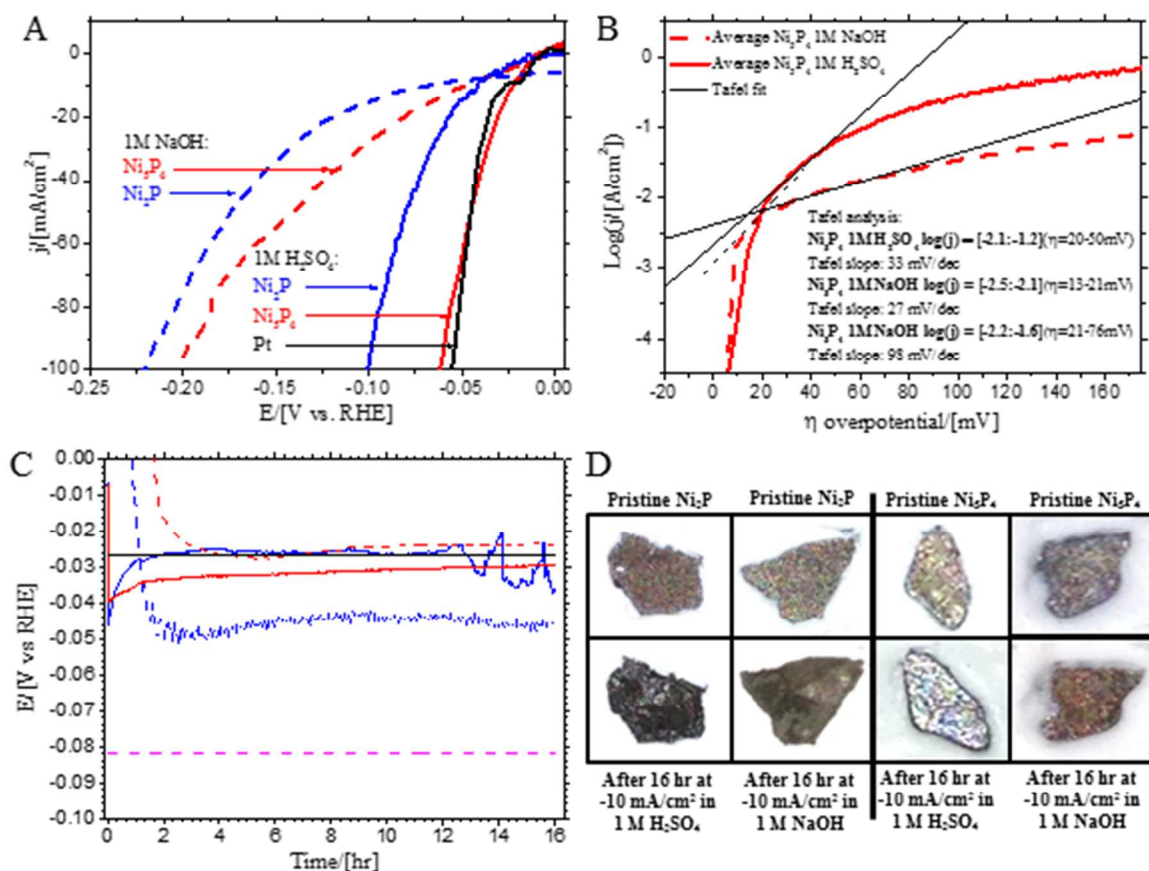


Fig. 3 Electrochemical analyses of  $\text{Ni}_5\text{P}_4$  MPs (red),  $\text{Ni}_2\text{P}$  NPs (blue), and Pt (black) in 1 M  $\text{H}_2\text{SO}_4$  (solid line) and 1 M NaOH (dashed line). Using a B-doped diamond counter electrode avoids any Pt contamination. All potentials are given against the reversible hydrogen electrode (RHE) (adjust for pH) and corrected for IR-drop (except Fig. 2C), for details see E.S.I (A) Voltammetry at 1 mV/s under 1 atm.  $\text{H}_2$ .  $\text{Ni}_5\text{P}_4$  is preconditioned at  $-10 \text{ mA/cm}^2$  for 16 hr prior to measurement. Pt and  $\text{Ni}_2\text{P}$  are measured for pristine catalysts due to temporal changes during CP analysis. Pt reference is measured at 100 mV/s due to diffusion limitations (see E.S.I). (B) Tafel analysis of  $\text{Ni}_5\text{P}_4$  MPs. See E.S.I for Tafel analysis of  $\text{Ni}_2\text{P}$  and Pt. (C) Chronopotentiometric (CP) analysis of both nickel phosphide materials in acid and base at  $-10 \text{ mA/cm}^2$  for 16 hr (non-IR corrected). The potential for the same kinetic current for Pt (black) (from this work) and for NiMo NPs (magenta), based on literature values<sup>26</sup>, are included for comparison. (D) Photographs of the  $\text{Ni}_5\text{P}_4$  and  $\text{Ni}_2\text{P}$  electrode surfaces before and after 16 hr CP analyses in 1 M  $\text{H}_2\text{SO}_4$  and 1 M NaOH.

1.4 m $\Omega$ . High frequency EIS measurements were used to estimate the uncompensated resistance at 12.4  $\Omega$  in 1 M  $\text{H}_2\text{SO}_4$ , which is  $10^4$  greater than the resistance to conduction through the pellet — thus indicating that the limiting resistance is from the solution not the electrode assembly. A polished Pt foil (Pt) served as a control (see ESI).

**2.2. Electrochemical Characterization:** Fig. 3A plots the voltammograms of pellet-electrodes made with  $\text{Ni}_2\text{P}$  NPs or  $\text{Ni}_5\text{P}_4$  MPs, compared to Pt foil in 1 M  $\text{H}_2\text{SO}_4$  or 1 M NaOH under 1 atm  $\text{H}_2$  gas. The potentials (vs. RHE) required to produce current densities of  $j = -10$  and  $-100 \text{ mA/cm}^2$  and Tafel slopes are summarized in Table 1.  $\text{Ni}_5\text{P}_4$  MPs were preconditioned at  $j = -10 \text{ mA/cm}^2$  for 16 hr prior to measurements. In contrast, both Pt and  $\text{Ni}_2\text{P}$  NPs were measured using pristine samples due to poisoning or corrosion instability, respectively, for these samples. For  $\text{Ni}_5\text{P}_4$  MPs the

potential (mV vs. RHE) required for  $j = -10 \text{ mA/cm}^2$  in 1 M acid is  $-23$  vs.  $-42$  for  $\text{Ni}_2\text{P}$  NPs, and  $-27$  for Pt. This performance difference is maintained at  $-100 \text{ mA/cm}^2$  (Fig. 3A). In 1 M alkali, the potentials increase relative to acid, but still favors  $\text{Ni}_5\text{P}_4$  MPs over  $\text{Ni}_2\text{P}$  NPs; the values at  $j = -10 \text{ mA/cm}^2$  are  $-49$ ,  $-69$ , &  $-82 \text{ mV}$  for  $\text{Ni}_5\text{P}_4$ ,  $\text{Ni}_2\text{P}$ , and NiMo NPs<sup>26</sup>, respectively. This performance difference is maintained at  $-100 \text{ mA/cm}^2$  and is actually better than  $\text{Ni}_2\text{P}$  NPs (1 mg/cm<sup>2</sup> thin-film) in the literature<sup>8</sup>, attributable to the increased loading (177 mg/cm<sup>2</sup>).

Fig. 3B plots the logarithm of current density vs. overpotential ( $\eta$ ) from which the slope (electrical potential cost per decade of current) reveals the HER kinetics (Tafel slope). We performed the Tafel analysis for  $\text{Ni}_5\text{P}_4$  MPs, Pt, and  $\text{Ni}_2\text{P}$  NPs in the interval  $-Tafel\ slope/2 < \eta < -Tafel\ slope$ , as recommended by Sheng et al.<sup>34</sup>. In acid electrolyte this yields differences of only 5–6 mV/dec, illustrating the similarities in reaction kinetics for

the 3 catalysts. Above this region, slopes increase as diffusion limitations begin to influence the Tafel kinetics. By contrast, in 1 M alkali the Tafel slope of Ni<sub>5</sub>P<sub>4</sub> MPs is 20 mV/dec smaller than of the Ni<sub>2</sub>P NPs. At larger applied potentials, Tafel slopes again increase as diffusion limitations begin to influence the kinetics. The Tafel slope of Ni<sub>2</sub>P NP pellet-electrodes agrees reasonably well with the Ni<sub>2</sub>P/Ti-foil-electrodes described by Popczun et al.<sup>8</sup> (see ESI). The Tafel slope of Ni<sub>5</sub>P<sub>4</sub> MPs in 1 M acid (33 mV/dec) and in 1 M base (98 mV/dec) should be compared to those for Pt (29 mV/dec, in acid) and bulk NiMo alloy (132 mV/dec, in base). Thus, the Tafel kinetics of Ni<sub>5</sub>P<sub>4</sub> MPs is essentially indistinguishable from the best reported values for the HER kinetics, *i.e.* Pt in acid and greatly improved over the bulk NiMo alloy in alkali.

Table 1. Performance of electrocatalysts.

Compound	Potential <sup>a</sup> required for $j = -10/-100$ mA/cm <sup>2</sup> / [mV vs. RHE]	Tafel slope / [mV/dec]	HER Faradaic efficiency, % H <sub>2</sub> yield	Estimated TOF / [mol H <sub>2</sub> / mol surface atoms / s] ( $\eta = 100$ mV / 200mV) <sup>b</sup>
Ni <sub>5</sub> P <sub>4</sub> (pellet)	-23/-62 (acid)	33 (acid)	100%±1% H <sub>2</sub> (acid) <sup>c</sup>	3.5/9.8 (acid)
	-49/-202 (base)	98 (base)	100%±5% H <sub>2</sub> (base) <sup>c</sup>	0.79/2.9 (base)
Ni <sub>2</sub> P (pellet)	-42/-101 (acid)	38 (acid)	unstable <sup>h</sup>	0.015/0.064 (acid) <sup>g</sup>
	-69/-220 (base)	118 (base)	unstable <sup>h</sup>	0.004/0.014 (base)
Bulk Pt foil	-27/-55 (acid)	29 (acid)	100%±2% H <sub>2</sub> (acid) <sup>f</sup>	329/(N/A) (acid)
NiMo alloy <sup>d</sup>	-82/(N/A) (base) <sup>26</sup>	132 (base) <sup>d</sup> <sub>35</sub>	N/A	0.05/0.36 (base) <sup>26,8</sup>

- Values are obtained from Fig. 2A, thus reflecting the kinetic current at 1 mV/s and not the steady state potentials.
- TOF was estimated by assuming all the catalyst was active, then normalization to the known value of Ni<sub>2</sub>P NP on Ti foil, to account for the lower active loading (see ESI for details).
- A second Tafel slope of 82 mV/dec is reported in literature at larger  $j$  values for Ni<sub>2</sub>P.
- Literature<sup>35</sup> NiMo Tafel slopes are reported for polycrystalline bulk alloy, whereas overpotentials and TOFs refer to NPs.
- H<sub>2</sub> and O<sub>2</sub> were determined by GC after passing 6 C (coulombs) in a one compartment cell (see ESI).
- Faradaic yield measurements were conducted on Pt/C/Nafion composites (see ESI).
- Popczun et al.<sup>8</sup> reports TOF = 0.015 s<sup>-1</sup> at  $\eta = 100$  mV and TOF = 0.5 s<sup>-1</sup> at 200 mV using NPs of Ni<sub>2</sub>P on Ti-foil.
- Ni<sub>2</sub>P corrodes during electrolysis, making long term H<sub>2</sub> yields time-dependent.

Far greater loadings of earth-abundant catalysts can be used compared to PGMs (Pt is more than 10<sup>3</sup> more expensive than Ni). Therefore, it is the geometric current density for earth-abundant catalysts which shows the true potential in applied energy harvesting. However, the intrinsic catalytic rate, albeit harder to determine, gives the activity of a single active site (turn-over frequency, TOF) and therefore is an alternative comparison to literature values. For new catalysts like the nickel phosphides—and indeed many earth-abundant catalysts—neither the nature of the active site nor its relative

abundance are known. Hence, we have adopted the method used by Popczun et al.<sup>8</sup> to estimate the number of catalytic sites per surface area (see ESI for method details) using the crystal structure, the BET surface area of the catalyst powder, and the activity at  $\eta=100$  mV and  $\eta=200$  mV. Using this method we arrived at an estimated 1.9·10<sup>15</sup> atoms per cm<sup>2</sup> of surface Ni<sub>5</sub>P<sub>4</sub> (2.0·10<sup>15</sup> atoms/cm<sup>2</sup> for Ni<sub>2</sub>P). For polished Pt foil we used the same method as for the nickel phosphides to estimate surface atom density, obtaining 4.1·10<sup>15</sup> surface atoms/cm<sup>2</sup>, close to the literature value of 1.5·10<sup>15</sup> surface atoms/cm<sup>2</sup> for Pt[111]<sup>36</sup>. Using the geometric surface area we obtained a TOF of 329 s<sup>-1</sup> for Pt foil.

Estimating the total electroactive surface area of catalyst in contact with the electrolyte is complicated for the solid pellet electrodes used here as they may be semi-porous. Initially, lower and upper bounds to the electrocatalytically active surface area were estimated assuming either the geometric surface area of the electrode or the volume of the full pellet (geometric area times the thickness of the solid pellet) times the measured N<sub>2</sub> BET surface areas (1m<sup>2</sup>/g for Ni<sub>5</sub>P<sub>4</sub> MPs and 69.4 m<sup>2</sup>/g for Ni<sub>2</sub>P NPs), neither of which were known to be the electrocatalytical area. Hence, to compare to literature reports we estimated the absolute TOFs by normalization of pellet electrodes to the reported TOF for thin-film Ni<sub>2</sub>P NPs<sup>8</sup>, for which the accurate active catalyst loading was known. This normalization was then applied to the Ni<sub>5</sub>P<sub>4</sub> MPs, as these could not be prepared as thin-films due to the high temperature transformation of Ni<sub>5</sub>P<sub>4</sub> to Ni<sub>2</sub>P. Table 1 compares the catalytic turnover frequencies (TOF) measured at 100 and 200 mV overpotentials for nickel phosphide pellets vs. other catalysts.

This comparison shows that the TOF of Ni<sub>5</sub>P<sub>4</sub> MPs exceeds that of Ni<sub>2</sub>P by 200 fold in both acid and base. Additionally, Ni<sub>5</sub>P<sub>4</sub> MPs have a 10 fold greater TOF than the previously reported values for state-of-the-art NiMo alloy<sup>8,26</sup>, with the latter TOFs 0.05 s<sup>-1</sup> and 0.36 s<sup>-1</sup> at  $\eta=100$  mV and  $\eta=200$  mV under alkaline conditions. The estimated TOF of Ni<sub>5</sub>P<sub>4</sub> MPs is about two orders of magnitude lower than that of the Pt-foil in acid at  $\eta = 100$  mV (assuming an atomically flat surface).

Steady-state activity and electrode degradation (corrosion) were investigated during 16 hr chronopotentiometric (CP) electrolysis at -10 mA/cm<sup>2</sup> in both acid and base. This current density has been widely adopted as a standard condition as it is equal to a photoelectrochemical cell operating at ~10 % solar efficiency<sup>37,38</sup>. Fig. 3C shows the time dependence of the CP potential of unconditioned pellet electrodes of Ni<sub>5</sub>P<sub>4</sub> and Ni<sub>2</sub>P foil (details in ESI). In acid, both Ni<sub>5</sub>P<sub>4</sub> MPs and Ni<sub>2</sub>P NPs exhibit short term increase in activity over ~2 hr to steady-state values (conditioning). The current for Ni<sub>2</sub>P NPs sometimes become unstable during 16 hr as shown (Fig. 3C) due to corrosion, which is in contrast to the stable current of Ni<sub>5</sub>P<sub>4</sub> MPs. In base, both Ni<sub>5</sub>P<sub>4</sub> MPs and Ni<sub>2</sub>P NPs exhibit conditioning over ~2 hr to steady-state values that favor Ni<sub>5</sub>P<sub>4</sub> by 21 mV after 16 hr. A similar trend, of smaller amplitude was reported previously for Ni<sub>2</sub>P NPs on Ti<sup>8</sup>. During electrolysis, Ni<sub>2</sub>P pellets physically degrade as seen by visible swelling and cracking of pellets (Fig. 3D), similar to the previous study<sup>8</sup>,

albeit with minimal potential change, see Fig. 3C. The reason for the apparent CP stability is the large amount of catalyst used to make electrode pellets. In contrast, the  $\text{Ni}_3\text{P}_4$  pellets retain their metallic luster and show little to no visible change, indicating stability against corrosion in both acid and base over 16 hr.

To corroborate the visual and electrochemical analysis of electrode stability, the electrolyte was sampled at time intervals and analyzed by ICP-MS elemental analysis for Ni (Fig. 4). This analysis shows no Ni dissolves from the  $\text{Ni}_3\text{P}_4$  electrode in 1 M NaOH over the 16 h electrolysis period. In 1 M  $\text{H}_2\text{SO}_4$  a sharp initial increase in dissolved Ni is observed that levels off at 14.3% within this same period. We attribute the initial loss in acid to the dissolution of other Ni products (residual precursor from the synthesis, or a surface layer of phosphate formed by air exposure) that does not dissolve in alkali. As this dissolution shows no correlation with the catalytic activity of the electrode, we conclude that the active  $\text{Ni}_3\text{P}_4$  MP sample is stable during  $\text{H}_2$  evolution. For comparison, an electrode pressed from  $\text{Ni}_2\text{P}$  NPs was investigated in 1 M  $\text{H}_2\text{SO}_4$ . As expected from the visual and electrochemical analysis, significant dissolution (50.5% after ~19 hr) was observed for this sample.

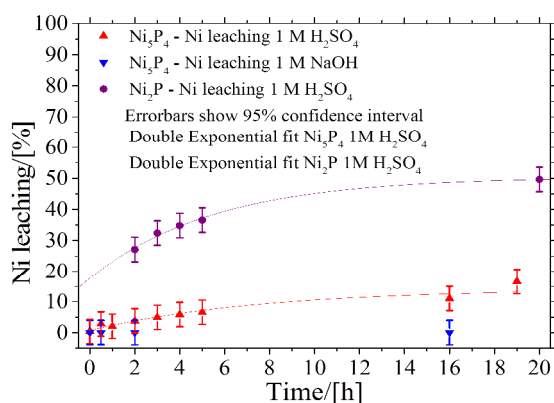


Fig. 4 Amount of Ni in the electrolyte during CP analysis in both acid and alkali. For comparison  $\text{Ni}_2\text{P}$  in acid is also shown. Method details see ESI.

**2.3. Post electrolysis characterization:** Lastly, Fig. 5 shows HRTEM images of particles obtained from the surface layer of an  $\text{Ni}_3\text{P}_4$  MP electrode after 6 hr of electrolysis in acid (A) and base (B) vs. before electrolysis (C). The particles show no visible sign of surface reconstruction and the presence of the amorphous carbon coating before and after catalysis indicates that particle size and shape are retained. Six lattice spacings compiled from multiple locations in both acid and base electrolyzed samples were found to agree well with the lattice spacings for  $\text{Ni}_3\text{P}_4$  from PXRD (see ESI), while not agreeing with any of the other low temperature nickel phosphide or nickel oxide phases, thus precluding the formation of new phases. Surface analysis by SEM-EDXS at multiple locations gave the average composition:  $\text{Ni}_{5.00}\text{P}_{4.19}$  and  $\text{Ni}_{5.02}\text{P}_{4.20}$  after electrolysis in acid and base, respectively, further confirming

retention of the initial catalyst composition. SEM images also corroborate the unchanged range of particle sizes and morphology between samples electrolyzed in acid and base (see Fig. 5(D) and (E)). All lines of evidence indicate chemical and electrochemical stability of  $\text{Ni}_3\text{P}_4$  in both acid and base.

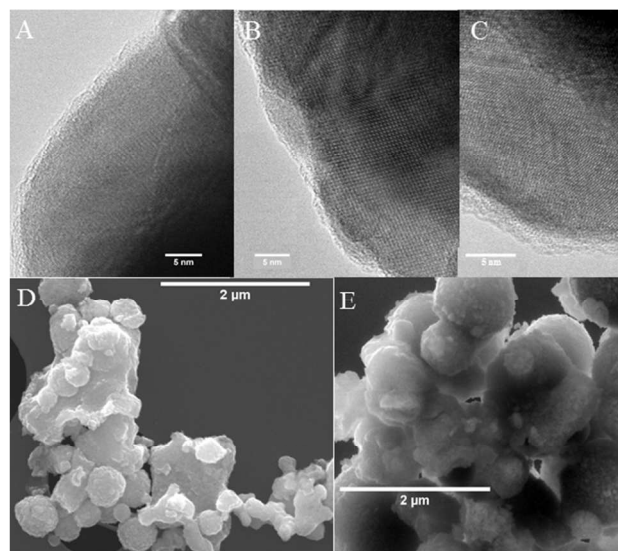


Fig. 5 HRTEM after 6 hr CP analysis at  $-10 \text{ mA/cm}^2$  in (A) 1 M  $\text{H}_2\text{SO}_4$  and (B) 1 M NaOH, and (C) shows  $\text{Ni}_3\text{P}_4$  before CP analysis, scale bar 5 nm. SEM images after 6 hr CP analysis at  $-10 \text{ mA/cm}^2$  in (D) 1 M  $\text{H}_2\text{SO}_4$  and (E) 1 M NaOH, scale bar 2  $\mu\text{m}$ .

### 3. Discussion:

The observed Tafel slope of 33 mV/dec in acid for  $\text{Ni}_3\text{P}_4$  MPs can be compared to theoretical expressions derived for  $\text{H}_2$  formation kinetics on an idealized planar surface having a single catalytic site in aqueous acid (such as crystalline Pt)<sup>39</sup>. Within the experimental uncertainty, the measured Tafel slope is comparable to the limiting Tafel slopes of 29 and 39 mV/dec. By contrast, a Tafel slope of 118 mV/dec is theoretically predicted when the RLS is the capture of a hydronium ion from solution and an electron from the metal conducting band onto an empty site (the discharge reaction), which therefore can be excluded as the RLS.

According to previously published electronic structure calculations (DFT) on  $\text{Ni}_2\text{P}$  [110], the HER mechanism in acid could proceed in three steps as shown in Fig. 6A. The first step (I) is the energetically favored electron transfer to a proton bound to a trigonal  $\text{Ni}_3$  site, the second step (II) is an electron transfer to a bridging proton at a Ni–P bond—this step was identified as being the rate-determining HER step<sup>28</sup>. The nature of the RDS suggests that the Ni–P bond length could be a reasonable reactivity descriptor—as increase of this bond length will favor greater electron localization on the P and therefore reduce the barrier to proton binding (greater basicity than Ni).

Fig. 6B and C show the relevant Ni–P bond lengths on the Ni<sub>2</sub>P [001] surface and for a similar site in the Ni<sub>5</sub>P<sub>4</sub> [001] direction (obtained from the ICSD verified PXRD structure). The Ni–P bond length increases to 2.306 Å in Ni<sub>5</sub>P<sub>4</sub> from 2.201 Å in Ni<sub>2</sub>P. By contrast, the Ni–Ni bond length of the trigonal Ni<sub>3</sub> site contracts by a comparable amount to 2.563 Å in Ni<sub>5</sub>P<sub>4</sub> from 2.640 Å in Ni<sub>2</sub>P. This contraction in Ni<sub>5</sub>P<sub>4</sub> allows an increased overlap of the filled Ni valence orbitals with the hydrogen 1s orbital and thus increases the covalent interaction making the first electron transfer more favorable. Increasing the binding strength of the first hydrogen atom would either accelerate the reaction if the population of this intermediate increases, or slow the reaction if absorption is too strong causing a slower desorption of the H<sub>2</sub> product. Optimal kinetics for this system would be achieved when the two steps have comparable energy barriers. The concomitant increase in Ni–Ni and decrease in Ni–

In summary, we have shown that Ni<sub>5</sub>P<sub>4</sub> MPs exhibit exceptionally high TOFs, greater than that of Ni<sub>2</sub>P NPs in 1 M H<sub>2</sub>SO<sub>4</sub> and 1 M NaOH and the previously reported value for NiMo NPs in 1 M NaOH, in combination with low electrical impedance losses and high corrosion resistance during electrolysis. Ni<sub>5</sub>P<sub>4</sub> also exhibits indistinguishable rate-limiting kinetics compared to Pt in acid at low current densities. This combination of superior efficiency and stability in both strong acid and strong alkali is unique among earth-abundant HER electrocatalysts and makes Ni<sub>5</sub>P<sub>4</sub> a promising candidate for the future development of renewable H<sub>2</sub> via water splitting.

## 5. Experimental:

**5.1. Catalyst synthesis:** Nanoparticulate Ni<sub>2</sub>P and Ni<sub>5</sub>P<sub>4</sub> were synthesized by a solvothermal method starting from nickel acetate and tri-octylphosphine using octylether/oleylamine and tri-octylphosphine oxide as solvents. Details are given in ESI

**5.2. Electrochemical testing:** Electrochemical cells were pre-cleaned in piranha (1:3 35% H<sub>2</sub>O<sub>2</sub> and conc. H<sub>2</sub>SO<sub>4</sub>) and after chronopotentiometric testing of Pt, in aqua regia, prior to the piranha cleaning. CV and CP analyses were conducted in a three-compartment cell with glass-frit separating the compartments. A luggin compartment holds the reference electrode. A boron-doped diamond thin-film counter electrode (~1 cm<sup>2</sup>, elementsix) and a home-made Ag/AgCl (3 M KCl) reference electrode were used. The working compartment was purged with 1 atm. H<sub>2</sub> prior to and during measurements. Working electrodes were made from 50 mg nickel phosphide powder, pressed into pellets (6 mm diameter) under 5 tons, back-connected to Ti-foil with Ag-paste (SPI), attached to a copper wire, and sealed in a glass tube with Loctite Hysol 1C epoxy exposing an electrode area of ~0.02–0.04 cm<sup>2</sup>.

All electrochemical potentials are reported vs. the reversible hydrogen electrode (RHE) by measuring the open circuit potential of a clean Pt electrode under 1 atm. H<sub>2</sub> in the electrolyte of interest at each pH. Potentials measured by CV are further corrected for IR-drop, while CP measurements are corrected only for pH and reference potential (not uncompensated IR drop).

**5.3. Faradaic efficiency:** Product measurements are conducted in a 1 compartment cell using a B-doped diamond counter electrode in a two-electrode configuration. A charge of 6 C at 1.96 mA corresponding to j ~10–100 mA/cm<sup>2</sup> depending on the electrode area. Prior to measurements the electrode was preconditioned by passing 6 C at the above conditions, followed by Ar purging for ≥ 20 min. H<sub>2</sub> (and O<sub>2</sub>) in the headspace were quantified by gas chromatography (GC). Commercial Pt nanoparticles supported on Vulcan carbon and dispersed in Nafion composite was used for comparison of faradaic efficiencies (see ESI for this electrode preparation). The faradaic yields of 89–92% were obtained for Pt.

**5.4. Elemental analysis:** ICP-OES (Perkin-Elmer Optima 7100) was used for the elemental analysis of the electrolyte at selected times during CP measurement, this was used to determine the leaching of Ni from the Ni<sub>5</sub>P<sub>4</sub> and Ni<sub>2</sub>P pellet electrodes (see ESI for details).

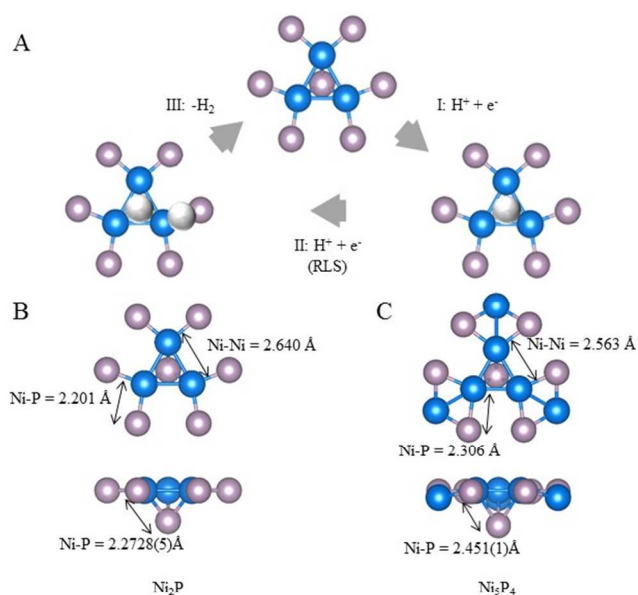


Fig. 6 (A) Schematic representation of the reaction mechanism suggested by Liu and Rodriguez<sup>28</sup> (B) Structural excerpt of the proposed active site on Ni<sub>2</sub>P [001] and (C) the

P bond lengths in Ni<sub>5</sub>P<sub>4</sub> relative to Ni<sub>2</sub>P are an indication of compensating  $\sigma+\pi$  electron transfer which is a signature of covalent bonding and shows that the two properties cannot be tuned individually. The effect of P basicity in the RLS is consistent with the observed Tafel slope excluding a discharge-type RLS—if the proton is interacting with the P prior to the RLS.

On this basis, and assuming the DFT inferred mechanism is correct, we suggest that Ni<sub>5</sub>P<sub>4</sub> possesses a faster rate due to increased binding energy of the first hydrogenic intermediate—which in turn increases the second proton affinity—accelerating the overall reaction rate compared to Ni<sub>2</sub>P.

## 4. Conclusion:

## Acknowledgements

The authors acknowledge funding from the AFOSR contract FA9550-11-1-0231, NATCO Pharma, NSF-MRSEC (DMR-0819860) to the Princeton Center for Complex Materials (N.Y.) for imaging facilities, and Rutgers University for a fellowship to ABL.

## Notes and references

<sup>a</sup> Department of Chemistry and Chemical Biology, Rutgers, the State University of New Jersey, 610 Taylor Road, Piscataway, 08854 New Jersey, USA

<sup>b</sup> PRISM Imaging and Analysis Center, Princeton University, 120 Bowen Hall, 70 Prospect Avenue, Princeton 08544, New Jersey, USA

<sup>c</sup> Department of Chemistry and Biochemistry, Rowan University, 201 Mullica Hill Road, Glassboro, New Jersey 08028, USA.

† Electronic Supplementary Information (ESI) available: Showing further synthesis and experimental details, PXRD, SEM, SEM-EDXS and TEM analysis and details, a.o. See DOI: 10.1039/b000000x/

- N. M. Marković, B. N. Grgur, and P. N. Ross, *J. Phys. Chem. B*, 1997, **101**, 5405–5413.
- P. C. K. Vesborg and T. F. Jaramillo, *RSC Adv.*, 2012, **2**, 7933–7947.
- A. B. Laursen, S. Kegnæs, S. Dahl, and I. Chorkendorff, *Energy Environ. Sci.*, 2012, **5**, 5577.
- D. Merki, S. Fierro, H. Vrubel, and X. Hu, *Chem. Sci.*, 2011, **2**, 1262.
- Y. Li, H. Wang, L. Xie, Y. Liang, G. Hong, and H. Dai, *J. Am. Chem. Soc.*, 2011, **133**, 7296–9.
- M. A. Lukowski, A. S. Daniel, F. Meng, A. Forticaux, L. Li, and S. Jin, *J. Am. Chem. Soc.*, 2013, **135**, 10274–7.
- W.-F. Chen, S. Iyer, S. Iyer, K. Sasaki, C.-H. Wang, Y. Zhu, J. T. Muckerman, and E. Fujita, *Energy Environ. Sci.*, 2013, **6**, 1818.
- E. J. Popczun, J. R. McKone, C. G. Read, A. J. Biacchi, A. M. Wiltrout, N. S. Lewis, and R. E. Schaak, *J. Am. Chem. Soc.*, 2013, **135**, 9267–70.
- Y. Xu, R. Wu, J. Zhang, Y. Shi, and B. Zhang, *Chem. Commun.*, 2013, **49**, 6656–6658.
- Z. Zhang, B. Lu, J. Hao, W. Yang, and J. Tang, *Chem. Commun. (Camb)*, 2014, **50**, 11554–7.
- Y. Liang, Q. Liu, A. M. Asiri, X. Sun, and Y. Luo, *ACS Catal.*, 2014, 4065–4069.
- J. F. Callejas, J. M. McEnaney, C. G. Read, J. C. Crompton, A. J. Biacchi, E. J. Popczun, T. R. Gordon, N. S. Lewis, and R. E. Schaak, *ACS Nano*, 2014.
- Z. Huang, Z. Chen, Z. Chen, C. Lv, H. Meng, and C. Zhang, *ACS Nano*, 2014.
- S. Cao, Y. Chen, C.-J. Wang, P. He, and W.-F. Fu, *Chem. Commun. (Camb)*, 2014, **50**, 10427–9.
- L. Feng, H. Vrubel, M. Bensimon, and X. Hu, *Phys. Chem. Chem. Phys.*, 2014, **16**, 5917–21.
- T. Burchardt, V. Hansen, and T. Våland, *Electrochim. Acta*, 2001, **46**, 2761–2766.
- Q. Liu, J. Tian, W. Cui, P. Jiang, N. Cheng, A. M. Asiri, and X. Sun, *Angew. Chemie*, 2014, **126**, 6828–6832.
- E. J. Popczun, C. G. Read, C. W. Roske, N. S. Lewis, and R. E. Schaak, *Angew. Chem. Int. Ed. Engl.*, 2014, **53**, 5427–5430.
- A. Lu, Y. Chen, H. Li, A. Dowd, M. B. Cortie, Q. Xie, H. Guo, Q. Qi, and D.-L. Peng, *Int. J. Hydrogen Energy*, 2014, **39**, 18919–18928.
- P. Xiao, M. A. Sk, L. Thia, X. Ge, R. J. Lim, J.-Y. Wang, K. H. Lim, and X. Wang, *Energy Environ. Sci.*, 2014, **7**, 2624.
- X. Chen, D. Wang, Z. Wang, P. Zhou, Z. Wu, and F. Jiang, *Chem. Commun. (Camb)*, 2014, **50**, 11683–5.
- Z. Xing, Q. Liu, A. M. Asiri, and X. Sun, *Adv. Mater.*, 2014, **26**, 5702–7.
- J. M. McEnaney, J. C. Crompton, J. F. Callejas, E. J. Popczun, A. J. Biacchi, N. S. Lewis, and R. E. Schaak, *Chem. Mater.*, 2014, **26**, 4826–4831.
- J. M. McEnaney, J. C. Crompton, J. F. Callejas, E. J. Popczun, C. G. Read, N. S. Lewis, and R. E. Schaak, *Chem. Commun. (Camb)*, 2014, **50**, 11026–8.
- M. S. Faber and S. Jin, *Energy Environ. Sci.*, 2014, **7**, 3519–3542.
- J. R. McKone, B. F. Sadtler, C. A. Werlang, N. S. Lewis, and H. B. Gray, *ACS Catal.*, 2012, **3**, 166–169.
- M. L. Helm, M. P. Stewart, R. M. Bullock, M. R. DuBois, and D. L. DuBois, *Sci.*, 2011, **333**, 863–866.
- P. Liu and J. A. Rodriguez, *J. Am. Chem. Soc.*, 2005, **127**, 14871–14878.
- Y. Lu, J.-P. Tu, Q.-Q. Xiong, J.-Y. Xiang, Y.-J. Mai, J. Zhang, Y.-Q. Qiao, X.-L. Wang, C.-D. Gu, and S. X. Mao, *Adv. Funct. Mater.*, 2012, **22**, 3927–3935.
- J. Ma, S. Ni, X. Lv, X. Yang, and L. Zhang, *Mater. Lett.*, 2014, **133**, 94–96.
- K. Aso, A. Hayashi, and M. Tatsumisago, *Inorg. Chem.*, 2011, **50**, 10820–10824.
- E. Muthuswamy, G. H. L. Savithra, and S. L. Brock, *ACS Nano*, 2011, **5**, 2402–2411.
- M. Yamamoto, K. Shirai, and K. Hiramatsu, *Jpn. J. Appl. Phys.*, 1991, **30**, 1036–1038.
- W. Sheng, H. A. Gasteiger, and Y. Shao-Horn, *J. Electrochem. Soc.*, 2010, **157**, B1529.
- J. . Jakšić, M. . Vojnović, and N. . Krstajić, *Electrochim. Acta*, 2000, **45**, 4151–4158.
- T. F. Jaramillo, K. P. Jørgensen, J. Bonde, J. H. Nielsen, S. Horch, and I. Chorkendorff, *Science*, 2007, **317**, 100–2.
- Z. Chen, T. F. Jaramillo, T. G. Deutsch, A. Kleiman-Shwarsstein, A. J. Forman, N. Gaillard, R. Garland, K. Takanebe, C. Heske, M. Sunkara, E. W. McFarland, K. Domen, E. L. Miller, J. A. Turner, and H. N. Dinh, *J. Mater. Res.*, 2011, **25**, 3–16.
- S. Hu, M. R. Shaner, J. A. Beardslee, M. Lichterman, B. S. Brunschwig, and N. S. Lewis, *Science (80-. )*, 2014, **344**, 1005–1009.
- J. O. Bockris and E. C. Potter, *J. Electrochem. Soc.*, 1952, **99**, 169.

Water splitting, powered by renewable electricity, is promising for producing clean hydrogen. Unfortunately, renewable energy coming from either sunlight or wind power is ill correlated with consumer demand, hence requiring storage, *e.g.* as a fuel in the form of hydrogen. Water splitting may be carried out electrocatalytically in electrolyzers using electricity from photovoltaics or wind power. However, acidic electrolyzers use scarce PGM metal catalysts (often Pt) for the hydrogen evolution reaction (HER). Although platinum is highly efficient, research efforts are directed towards replacing this catalyst with more earth abundant materials. State of the art alkaline electrolyzers use Ni-based catalysts but show lower efficiencies due to inefficient catalysis and therefore have high operating costs. Recently, transition metal phosphides, especially of Ni and Co, have been shown to be promising for the replacement of platinum in acidic solutions. While these materials are cheap, abundant, and active for the HER, not all forms are stable during catalysis. This paper shows that a new member of this family,  $\text{Ni}_5\text{P}_4$ , show an excellent activity, not only in acid, but also in alkali as well as being stable during electrolysis.